

Transverse modes in oxide confined VCSELs: Influence of pump profile, spatial hole burning, and thermal effects

C. Degen, I. Fischer and W. Elsässer

*Institute of Applied Physics, Darmstadt University of Technology,
Schloßgartenstr. 7, D-64289 Darmstadt, Germany*

christian.degen@physik.tu-darmstadt.de

Abstract: We present experimental studies on the transverse mode emission behaviour of oxide-confined Vertical Cavity Surface Emitting Lasers (VCSELs). VCSELs with aperture diameters of $6\mu\text{m}$ and $11\mu\text{m}$ exhibit a wide variety of emission patterns from low order Hermite-Gaussian modes to high order Laguerre-Gaussian modes. We obtain detailed information about the spatial gain distribution by recording spontaneous emission intensity profiles during lasing operation. We conclude from these profiles, that the spatial carrier distribution is primarily governed by the influence of pump induced current spreading and is only secondarily influenced by further effects such as spatial hole burning, and thermal gradients in the laser. The combination of these mechanisms causes a strong tendency towards the emission of high order transverse modes.

©1999 Optical Society of America

OCIS codes: (140.0140) Lasers and laser optics; (140.2020) Diode lasers; (140.5960) Semiconductor lasers; (250.7260) Vertical cavity surface emitting lasers

References

1. K. J. Ebeling, U. Fiedler, R. Michalzik, G. Reiner and B. Weigl, "Efficient Vertical Cavity Surface Emitting Laser Diodes for High Bit Rate Optical Data Transmission," *Int. J. Electron. Commun.* **50**, 316-326 (1996).
2. C. Degen, J.-L. Vey, W. Elsässer, P. Schnitzer and K. J. Ebeling, "Amplitude noise squeezed light from a polarisation single mode VCSEL," *Electron. Lett.* **34**, 1585-1586 (1998).
3. C. J. Chang-Hasnain, M. Orenstein, A. Von Lehmen, L. T. Florez, J. P. Harbison and N. G. Stoffel, "Transverse mode characteristics of vertical cavity surface-emitting lasers," *Appl. Phys. Lett.* **57**, 218-220 (1990).
4. C. J. Chang-Hasnain, J. P. Harbison, G. Hasnain, A. C. Von Lehmen, L. T. Florez and N. G. Stoffel, "Dynamic, Polarization, and Transverse Mode Characteristics of Vertical Cavity Surface Emitting Lasers," *IEEE J. Quantum Electron.* **27**, 1402-1409 (1991).
5. I. Hörsch, R. Kusche, O. Marti, B. Weigl and K. J. Ebeling, "Spectrally resolved near-field mode imaging of vertical cavity semiconductor lasers," *J. Appl. Phys.* **79**, 3831-3834 (1996).
6. H. Li, T. L. Lucas, J. G. McInerny and R. A. Morgan, "Transverse Modes and Patterns of Electrically Pumped Vertical-cavity surface-emitting Semiconductor Lasers," *Chaos, Solitons & Fractals* **4** (1994).
7. Y. G. Zhao and J. McInerny, "Transverse-Mode Control of Vertical-Cavity Surface-Emitting Lasers," *IEEE J. Quantum Electron.* **32**, 1950-1958 (1996).
8. W. Nakwaski and R. P. Sarzala, "Transverse modes in gain-guided vertical-cavity surface-emitting lasers," *Opt. Commun.* **148**, 63-69 (1998).
9. J. Wilk, R. P. Sarzala and W. Nakwaski, "The spatial hole burning effect in gain-guided vertical-cavity surface-emitting lasers," *J. Phys. D: Appl. Phys.* **31**, L11-L15 (1998).
10. K. L. Lear, K. D. Choquette, R. P. Schneider, Jr. and S. P. Kilcoyne, "Modal analysis of a small surface emitting laser with a selectively oxidized waveguide," *Appl. Phys. Lett.* **66**, 2616-2618 (1995).

11. D. L. Huffaker, D. G. Deppe and T. J. Rogers, "Transverse mode behaviour in native-oxide-defined low threshold vertical-cavity lasers," *Appl. Phys. Lett.* **65**, 1611-1613 (1994).
 12. C. Jung, R. Jäger, M. Grabherr, P. Schnitzer, R. Michalzik, B. Weigl, S. Müller and K. J. Ebeling, "4.8mW singlemode oxide confined top-surface emitting vertical-cavity laser diodes," *Electron. Lett.* **33**, 1790-1791 (1997).
 13. J. E. Epler, S. Gehrsitz, K. H. Gulden, M. Moser, H. C. Sigg and H. W. Lehmann, "Mode behaviour and high resolution spectra of circularly-symmetric GaAs-AlGaAs air-post vertical cavity surface emitting lasers," *Appl. Phys. Lett.* **69**, 722-724 (1996).
 14. S. F. Pereira, M. B. Willemsen, M. P. van Exter and J. P. Woerdman, "Pinning of daisy modes in optically pumped vertical-cavity surface-emitting lasers," *Appl. Phys. Lett.* **73**, 2239-2241 (1998).
 15. W. Nakwaski, "Current spreading and series resistance of proton-implanted vertical-cavity top-surface-emitting lasers," *Appl. Phys. A* **61**, 123-127 (1995).
 16. D. Vakhshoori, J. D. Wynn and G. J. Zydzik, "Top-surface emitting lasers with 1.9 V threshold voltage and the effect of spatial hole burning on their transverse mode operation and efficiencies," *Appl. Phys. Lett.* **62**, 1448-1450 (1993).
 17. G. C. Wilson, D. M. Kuchta, J. D. Walker and J. S. Smith, "Spatial hole burning and self-focussing in vertical-cavity surface-emitting laser diodes," *Appl. Phys. Lett.* **64**, 542-544 (1994).
-

1. Introduction

Vertical Cavity Surface Emitting Lasers (VCSELs) are well established devices used in manifold commercial [1] and scientific [2] applications. Their advantages over edge-emitting lasers are a high modulation bandwidth, simple array integration, low threshold currents, and longitudinal single mode emission. Furthermore, the circular symmetric cavity exhibits round and astigmatism-free beams, which is advantageous in fiber-coupling applications. However, high fiber-coupling efficiencies are only reached at low optical powers, because with increasing output power, higher order transverse modes are supported by the cavity due to the two-dimensional extension of the mirrors. In general, the complex transverse modal behaviour of VCSELs at high pump rates is a major drawback for many practical applications. The modal behaviour, just like most of the other key properties of the VCSELs, depends strongly on the confinement mechanism. The first available devices were air-post VCSELs with strong index-guiding by a step-like index profile of etched mesas. Lower threshold currents and higher efficiencies can be achieved with proton implanted devices. In these VCSELs, a ring-shaped area of low electrical conductivity at the periphery of the VCSEL causes the confinement of the injection current which leads to predominant gain guiding. These proton implanted VCSELs represented for quite a long time the state-of-the-art devices and consequently, manifold experimental [3,4,5,6] and theoretical [7,8,9] investigations have been performed on the nearfield distributions and modal dynamics of these VCSELs. The most recent development is the realization of gain-guiding by selective oxidization of Al-containing layers in the stack of the top Bragg-mirror. This technique enables a further reduction of the threshold current by a more efficient carrier confinement. On the other hand, the Al_xO_y layers also influence the optical field in the cavity by their reduced index of refraction. Thus, the optical field in a selectively oxidized VCSEL is simultaneously governed by carrier confinement by the oxide layer, interaction of the optical field with the carrier reservoir (spatial hole burning) and further mechanisms such as guiding by thermal lensing or weak index guiding by the oxide layer. The complex interplay of these effects is the reason, why an analysis of the transverse mode characteristics of oxide confined VCSELs has been so far restricted to nonlasing modes [10] or to low pump rates [11] in square aperture VCSELs.

In this contribution, we present the first detailed experimental investigations of the transverse modal behaviour of round aperture oxide confined VCSELs for a wide

range of injection currents even well above the thermal roll-over. We show images of the optical nearfield of $6\mu\text{m}$ and $11\mu\text{m}$ aperture diameter VCSELs. The lasers show a wide variety of transverse modes from low order Hermite-Gaussian modes to high order Laguerre-Gaussian modes. The large aperture laser even supports 18-lobed daisy modes. Furthermore, we present spontaneous emission intensity profiles measured under lasing operation and at wavelengths far away from the lasing wavelength. Thus, these profiles represent the spatial carrier distribution in the active region during lasing operation. A comparison of the carrier distribution with the lasing nearfield enables us to clearly distinguish different interacting mechanisms in the laser. We find, that inhomogeneities in the pump profile dominate the transverse emission properties, whereas spatial hole burning only weakly modifies the carrier profile. This is clearly evident from the spontaneous emission profiles. At high pump rates, the influence of thermal gradients inside the cavity becomes stronger which leads to a further preference of high order modes. The emission of high order daisy modes is a consequence of this effect. Our interpretation of the experimental data for the oxide confined VCSEL is in surprisingly good agreement with the results of recent theoretical modelling for proton-implanted VCSELs [7,8].

The paper is organized as follows: The experimental setup and structural information on the VCSELs are presented in section 2. In section 3, we show nearfield images of two VCSELs and spontaneous emission profiles for different pump rates. The different contributions to the profiles are then discussed in section 4 and our interpretation is compared with theoretical predictions. The last section summarizes the results of this paper.

2. Experimental setup and VCSEL structures

We record images of the intensity distributions of the lasing nearfield and of spontaneous emission of the VCSEL during lasing operation in order to obtain information about the transverse mode structure and spatial carrier distribution. The experimental setup for the recording of the nearfield images is shown in Fig. 1.

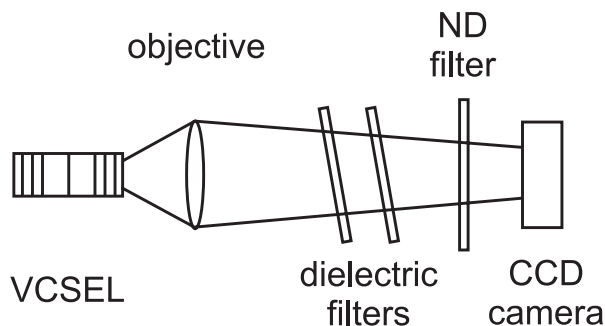


Figure 1. Experimental setup

The nearfield of the VCSELs is projected onto a CCD-camera by using a 14.5 mm focal distance collimating objective (Melles-Griot). Neutral density filters of various extinction ratios adapt the intensity of the laser nearfield to the sensitivity of the CCD-camera.

The spatial distribution of the spontaneous emission during lasing operation is recorded with the same setup. For this purpose, the lasing modes are blocked by two interference filters, each single filter of rejection ratio 10^4 . The filters are tuned to the next transparency wavelengths of the VCSELs' Bragg-mirrors below and above the lasing wavelength ($\lambda \approx 800..807\text{nm}$), which are at $\lambda \approx 770\text{nm}$ and $\lambda \approx 835\text{nm}$,

respectively. These spontaneous emission patterns are then directly recorded with the CCD-camera without any neutral density filters.

The lasers under investigation are oxide confined GaAs top-emitting VCSELs. They were fabricated at the University of Ulm. More details about the structure of the lasers can be found in [12]. Our devices only differ in the diameter of the oxide aperture, which amounts to $6\mu\text{m}$ and $11\mu\text{m}$, respectively. The VCSELs are operated ‘on-wafer’, using a needle-contact in order to inject the pumping current, which is delivered by a conventional constant current source. The wafer is mounted on a copper plate, which is actively stabilized at room temperature. The lasers emit at a wavelength of $\lambda \approx 800..807\text{nm}$. The optical power versus injection current characteristics of both VCSELs are shown in Fig. 2, with the pump rate $R_p = (I - I_{th})/I_{th}$ given on the top abscissa axis. The lasers show a pronounced thermal roll-over behaviour which is a characteristic for VCSELs. Threshold currents amount to $I_{th} = 2\text{mA}$ ($6\mu\text{m}$ diameter VCSEL) and to $I_{th} = 7\text{mA}$ ($11\mu\text{m}$ diameter VCSEL), maximum output powers to $P_{max} = 4.1\text{mW}$ and $P_{max} = 5.6\text{mW}$ at pump rates of $R_p = 5$ and $R_p = 2$, respectively.

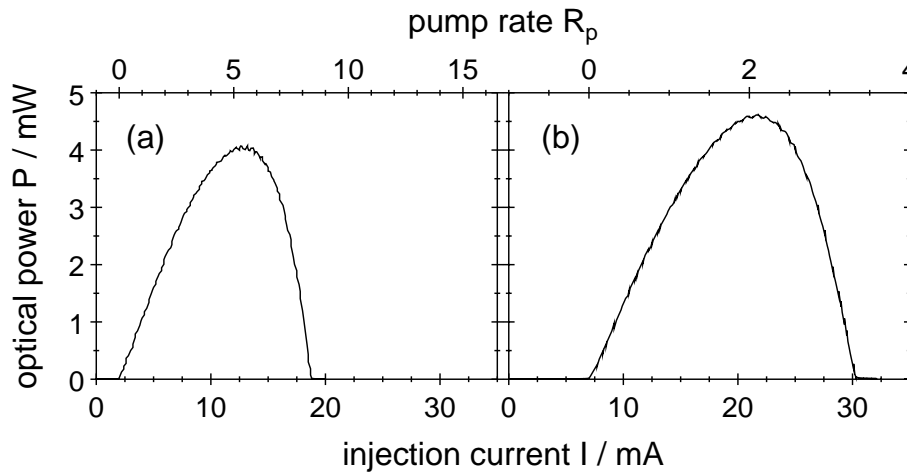


Figure 2. Optical power vs. injection current for VCSELs of $6\mu\text{m}$ (a) and $11\mu\text{m}$ (b) aperture diameter

3. Nearfield images and spontaneous emission profiles

3.1 Small aperture VCSEL

Nearfield images of the $6\mu\text{m}$ aperture diameter VCSEL are presented in Fig. 3. The images are coded in a ‘rainbow-like’ colour scheme, with the highest intensity corresponding to red and the lowest intensity corresponding to black. Figure 3 contains images for injection currents of 3.0mA (a), 6.2mA (b), 14.7mA (c), and 18mA (d).

At $I=3.0\text{mA}$, which corresponds to a low pump rate of $R_p = 0.5$, the VCSEL emits in the fundamental transverse mode, which is a Hermite-Gaussian TEM_{00} mode.

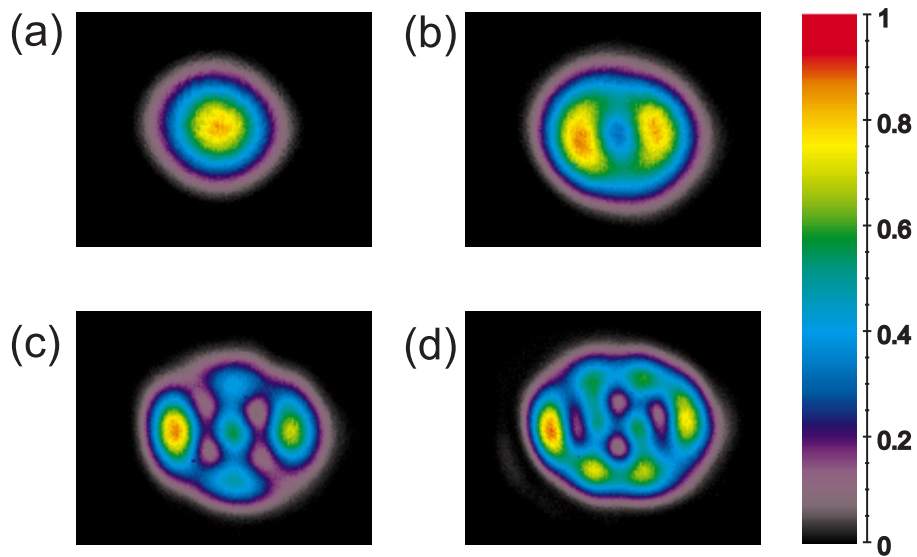


Figure 3. Nearfield images of the $6\mu\text{m}$ VCSEL at injection currents of 3.0mA (a), 6.2mA (b), 14.7mA (c), and 18mA (d)

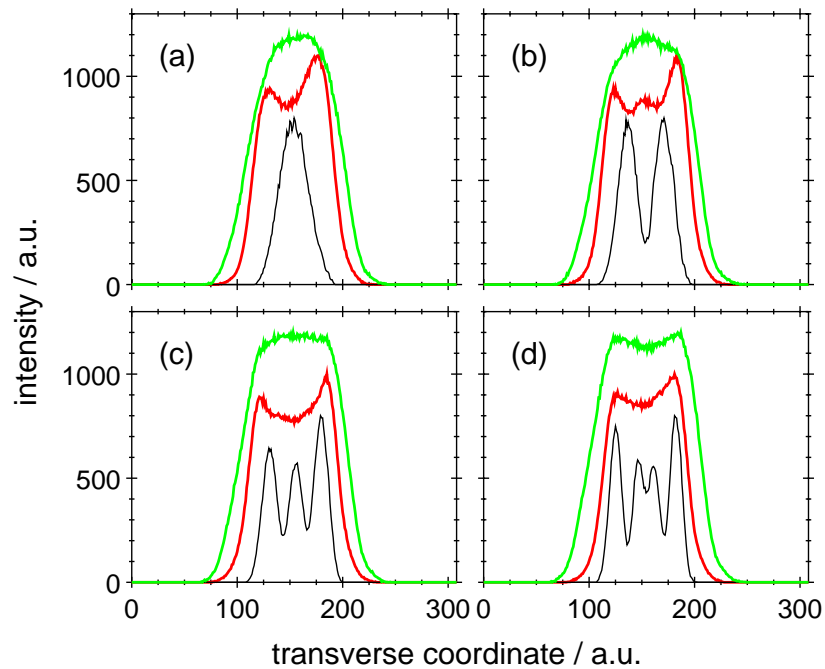


Figure 4. Transverse distribution of the laser intensity at $\lambda \approx 800\text{nm}$ (black curve), spontaneous emission at $\lambda \approx 770\text{nm}$ (red curve), and spontaneous emission at $\lambda \approx 830\text{nm}$ (green curve) of a $6\mu\text{m}$ VCSEL for injection currents $I=3\text{mA}$ (a), $I=6\text{mA}$ (b), $I=15\text{mA}$ (c), and $I=18\text{mA}$ (d)

With increased injection current of 6.2mA ($R_p = 2.1$), the nearfield distribution contains both a high intensity TEM_{10} mode and a lower intensity TEM_{01} mode. A similar superposition of modes of the first TEM mode family has already been reported e.g. by Epler et. al. [13] for the case of an $12\mu\text{m}$ air-post VCSEL. They showed the composition of a doughnut-shaped TEM_{01*} mode of a TEM_{10} and a TEM_{01} mode of similar intensities. However, in Fig.3 the nearfield image is clearly asymmetric due to different intensities of the two TEM modes. Higher order Hermite-Gaussian modes are present in the nearfield image for the next higher injection current, namely a bright TEM_{20} mode and a low intensity TEM_{02} mode. Note that at this injection current, the L-I curve of the VCSEL has already a negative slope. As a consequence, the laser's optical output power is drastically reduced to only 0.5mW by further increasing the injection current to $I=18\text{mA}$ ($R_p = 8$). The nearfield at this pump rate can be decomposed into a TEM_{30} and a TEM_{12} mode. The maxima of these modes are washed out due to the presence of even further, weakly excited higher order modes.

The profiles in Fig.4 are transverse cuts through the intensity distributions of the lasing emission at $\lambda \approx 800\text{nm}$ (black curve), spontaneous emission at $\lambda \approx 770\text{nm}$ (red curve), and spontaneous emission at $\lambda \approx 830\text{nm}$ (green curve) of the $6\mu\text{m}$ VCSEL for four injection currents. All curves give relative intensity values in order to take advantage of the whole dynamical range of CCD-camera and graphical representation. The two profiles of the spontaneous emission intensity directly reflect the spatial distribution of carriers at an energy higher than the lasing transition (High Energy Carrier Distribution, *HECD*) and of the carriers at an energy level below the energy of the lasing transition (Low Energy Carrier Distribution, *LECD*).

In Fig.4a, a smooth, broad profile with a maximum in the center of the VCSEL is observed for the LECD for a low pump rate of $R_p = 0.5$ ($I=3\text{mA}$). In contrast, the HECD curve shows a minimum at the center which is surrounded by distinct peaks. This minimum in the HECD coincides spatially with the maximum of the Gaussian-like intensity profile of the lasing field. At higher currents (Fig.4b), the single peak in the LECD becomes broader, whereas the HECD shows a 'negative fingerprint' of the lasing field: In the center of the VCSEL, two local minima of the HECD can be clearly recognized. These minima in the HECD coincide spatially with the maxima of the lasing nearfield distribution whereas the maximum in the center of the HECD coincides with the minimum in the nearfield. Furthermore, the side-maxima are more pronounced and narrower as compared to low current conditions and move towards the periphery of the laser. With further increasing pump rate (Fig.4c), the LECD again becomes broader and exhibits a plateau, whereas the side-maxima in the HECD move further towards the sides. The optical power is reduced as compared to Fig.4b. Thus, an influence of single peaks in the lasing profile on the HECD cannot be observed in this image. In Fig.4d, both HECD and LECD show a similar profile with a broad dip in the center. The intensity difference between the maxima and the minimum in the center ('contrast') of the HECD is reduced in comparison to Fig.4c. An influence of the lasing nearfield profile on the carrier profiles cannot be seen. However, it is striking that the maxima of the lasing field are at the same transverse coordinate as the maxima of the carrier distributions.

The connection between the carrier distribution and the lasing modes for both, the $6\mu\text{m}$ and the $11\mu\text{m}$ VCSEL will be discussed in section 4.

3.2 Large aperture VCSEL

The lasing nearfield distribution of a $11\mu\text{m}$ aperture diameter VCSEL is shown in Fig.5, using the same colour coding as in Fig.3. The injection currents amount to (a) 8.8mA ($R_p = 0.3$), (b) 15.5mA ($R_p = 1.2$), (c) 23.0mA ($R_p = 2.3$), and (d) 29.9mA ($R_p = 3.3$).

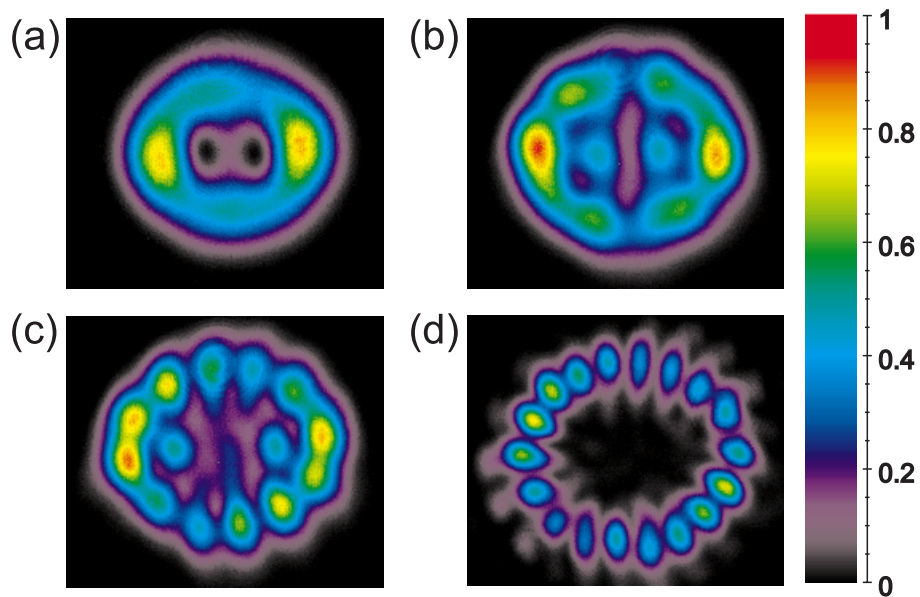


Figure 5. Nearfield images of the $11\mu\text{m}$ VCSEL at injection currents of 8.8mA (a), 15.5mA (b), 23.0mA (c) and 29.9mA (d)

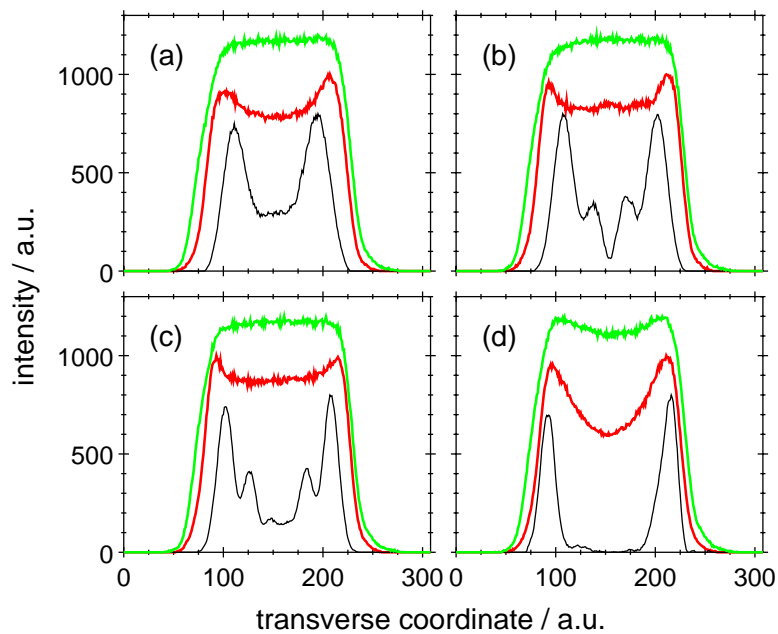


Figure 6. Transverse distribution of the optical laser field at $\lambda \approx 800\text{nm}$ (black), spontaneous emission at $\lambda \approx 770\text{nm}$ (red), and spontaneous emission at $\lambda \approx 830\text{nm}$ (green) of a $11\mu\text{m}$ VCSEL for injection currents $I=9\text{mA}$ (a), $I=15\text{mA}$ (b), $I=24\text{mA}$ (c), and $I=30\text{mA}$ (d)

The lowest order mode, which is emitted by the $11\mu\text{m}$ VCSEL, is the TEM_{10} mode at $I=7.2\text{mA}$ ($R_p = 0.03$). At only slightly higher currents, further modes appear, which is illustrated in Fig.5a. The nearfield image seems to contain a strong TEM_{10} and a weak TEM_{01} mode. However, there is a nonvanishing intensity at the center of the aperture, which indicates the presence of a TEM_{20} mode with suppressed central maximum instead of the TEM_{10} mode. This also explains the strong asymmetry of the nearfield image. The suppression of the central maximum in even-order Hermite-Gaussian modes is indeed predicted from numerical modelling of the mode distribution in a gain-guided VCSEL by Nakwaski et. al. [8]. Figure 5b offers a more complex modal behaviour. This distribution can be decomposed into TEM_{30} , TEM_{12} and weakly excited higher order modes, which form a faded background intensity. Furthermore, most of the laser intensity is now located at the periphery of the VCSEL. The nearfield shows even higher order modes in Fig.5c, which corresponds to $I = 23\text{mA}$ and already decreasing optical power. At this injection current, a TEM_{06} Laguerre-Gaussian mode and again a TEM_{20} Hermite-Gaussian mode with suppressed central maximum are emitted. The background intensity at the left and right borders of the laser again indicate the presence of higher order modes at this pump rate. In Fig.5d, a pure high order Laguerre-Gaussian mode TEM_{09} can be observed, which is usually attributed to as ‘daisy’ mode. To our knowledge, the only daisy mode of comparable order observed in a VCSEL so far was a 7th order mode reported by Pereira et. al. [14], who generated high order Laguerre-Gaussian modes by optically pumping an uniform VCSEL-wafer with a ‘doughnut’-shaped pump-profile. An 9th order mode in an electrically pumped VCSEL has not been reported so far. The emission of such high order modes even in an electrically pumped VCSEL is only possible if the processed wafer is of extraordinary homogeneity.

Transverse profiles of the intensity distribution in the $11\mu\text{m}$ VCSEL are presented in Fig. 6. Again, the black curves represent cuts through the lasing nearfields ($\lambda \approx 800\text{nm}$), the red curves are cuts through the profile of the spontaneous emission at $\lambda \approx 770\text{nm}$, representing the transverse high energy carrier distribution (HECD), whereas the green curves denote the spontaneous emission distribution at $\lambda \approx 830\text{nm}$, which reflects the low energy carrier profile (LECD).

Figure 6a depicts the carrier profiles at an injection current of $I=9\text{mA}$, corresponding to a pump rate of $R_p = 0.3$. At this pump rate, the LECD is nearly constant over most of the VCSELs diameter, while the HECD shows pronounced maxima at the wings of the curve, similar to the profiles of the $6\mu\text{m}$ VCSEL in Fig.4a. The profile of the lasing optical field also shows distinct peaks at the periphery, which are closer to the center than the maxima in the HECD. However, a direct influence of this lasing profile cannot be concluded from the HECD. A different situation is shown in Fig.6b for $I=15\text{mA}$ ($R_p = 1.1$). The LECD keeps its shape, but a weak influence of the lasing intensity profile on the HECD can be recognized. In between the side maxima of the HECD, which are narrower and move towards the periphery, a weak local maximum in the center of the VCSEL appears, which coincides with the minimum of the lasing field distribution. Furthermore, small dips in the HECD can be found at the same coordinates as the weak local maxima in the lasing distribution. At further increased injection current (Fig.6c), a direct modification of the carrier profiles by the lasing emission cannot be resolved, while the LECD remains at a stable plateau and the side-peaks in the HECD again become steeper and move further towards the periphery. Figure 6d shows a qualitatively similar behaviour as Fig.4d. The lasing intensity has almost decreased to zero and the peaks of the lasing field have moved far away towards the border of the laser where they coincide with strong maxima of the HECD and only weakly developed maxima of the LECD.

4. Discussion

In this section, our aim is to distinguish between the influences that different effects such as pump induced current spreading, spatial hole burning, and thermal gradients inside the cavity have on the carrier distribution. These complex and partly counter-acting effects then result in the preference of high order transverse modes in the optical nearfield.

We conclude from the results of section 3 that pump induced inhomogeneities predominantly govern the carrier distribution in the laser. These inhomogeneities arise purely from the current flow through the confinement area and not from an interaction with optical fields in the cavity. This conclusion is supported by the results of theoretical simulations by Nakwaski [15]. He performed numerical calculations on the transverse spreading of the injection current in proton-implanted VCSELs independently from the influence of optical fields inside the cavity. The modelling resulted in distributions of the current density inside the carrier confinement region, that showed distinct maxima at the borders of the VCSEL and a deep dip in the center. These distributions are in good agreement with the HECD profiles in Fig.4 and Fig.6. The HECD shows at all injection currents and for both VCSELs a corresponding shape with maxima at the periphery and a broad minimum in the center. This distribution causes obviously a strong tendency towards the emission of high order modes, which efficiently benefit from the inhomogeneous spatial gain distribution. The good agreement of the theoretical results for the proton implanted VCSEL and our experimental results obtained from oxide confined devices are quite remarkable since one of the major differences between these structures is the stronger carrier confinement by the oxide layers.

The tendency to high order mode emission is further enhanced by spatial hole burning and the effects of strong thermal gradients inside the cavity. The influence of these effects on the carrier distribution and on the lasing nearfield have been modelled in detail by Zhao et. al. [7] and by Nakwaski et. al. [8]. They simulated the carrier distribution and transverse emission characteristics in proton-implanted VCSELs with the restriction of their models to only the central part of the active region, which is equivalent to only low order transverse modes. Despite this restriction and the different confinement in our VCSELs, Zhao's results for the carrier distribution under influence of spatial hole burning are very similar to the HECDs in Fig.4b. There, in the central region of the VCSEL in between the pump induced maxima, two weak holes are burned in the HECD resulting in a carrier profile of the same shape as the one modelled by Zhao. Furthermore, the influence of spatial hole burning on the HECD is much smaller than the effect of current spreading, but it further enhances the tendency to higher order mode emission. In contrast to the modelling results, we find the spatial hole burning in the small VCSEL to be stronger than in the large VCSEL. This is not surprising, because in the $6\mu\text{m}$ aperture VCSEL, we have found power densities as much as 10 times higher than in the $11\mu\text{m}$ VCSEL. Thus, the higher power densities can obviously burn spatial holes of higher contrast as can be seen in comparison of Fig.4 and Fig.6. These observations yield further supplementary knowledge compared to the already reported experimental works on spatial hole burning in VCSELs [16,17], because these were restricted to low order transverse modes only, whereas our measurements show the influence of more complex nearfields on the spatial carrier distribution.

A third effect that forces the laser to high order mode emission is the presence of strong thermal gradients in the cavity. These gradients have also been modelled and temperature differences larger than 30K have been predicted between the center and the border region of the VCSEL [8]. These differences origin from Joule-heating and heating by non-radiating recombination processes. Thus, the temperature differences

will be highest for injection currents larger than the thermal roll-over point, because then the injection current is already high and non-radiating recombination strongly increases. As a consequence of this thermal gradient, carriers will be thermally excited and re-distributed towards higher energies. This effect of spectral carrier re-distribution is of course stronger in the hot center of the VCSEL and weaker at the cooler periphery. In a small energy interval, as it is selected by the interference filters at the wavelength of spontaneous emission but as well by the VCSELS' Bragg-reflector at the lasing wavelength, the strong re-distribution of carriers in the center of the VCSEL will obviously lead to a broad dip in the carrier distribution. This dip can be observed in Fig.4d and Fig.6d for both, HECD *and* LECD, the latter being free of the effects of current spreading or spatial hole burning at all other pump rates. We interpret this behaviour, especially the dip in the LECD, as a direct consequence of the strong thermal gradients. Only with this additional mechanism, a particularly tailored gain distribution can occur, that is very similar to the 'doughnut' shaped optically pumped setup by Pereira [14]. Consequently, very similar daisy-modes can be observed in this electrically pumped setup, with the order of the modes even exceeding the ones observed in the optically pumped VCSEL.

5. Summary

In conclusion, we have presented for the first time combined experimental studies on the transverse mode emission and the spatial carrier distribution in circular symmetric oxide confined VCSELS. The optical nearfields of VCSELS of $6\mu\text{m}$ and $11\mu\text{m}$ aperture diameter show a wide variety of modes, ranging from low order Hermite-Gaussian modes in the small aperture VCSEL to extremely high order Laguerre-Gaussian modes in the large aperture VCSEL for injection currents well above the thermal roll-over. We have discussed these modes in conjunction with the spatial distribution of the spontaneous emission intensity during lasing operation. We conclude from the results that pump induced current spreading in the confinement region is the dominant mechanism governing the spatial carrier distribution in the active region. This current spreading, in conjunction with additional effects such as spatial hole burning and thermal gradients in the cavity modify the carrier distribution in such a way, that the emission of high order transverse modes is strongly preferred. At high pump rates, the effect of spectral carrier re-distribution in the hot center of the VCSEL becomes so strong, that even a ring-shaped carrier distribution arises, which then leads to the emission of extremely high order modes, e.g. an 9th order daisy mode.

6. Acknowledgements

We gratefully acknowledge Prof. K.J. Ebeling and his group at the University of Ulm for providing us with their excellent VCSEL structures.